



Incremental Forming of the Al-Li Alloy AA2195: Role of Texture and Microstructure

A.M. MORE,¹ R. KALSAR,¹ P. SHIVASHANKAR,¹ R. LINGAM,²
N.V. REDDY,² O. PRAKASH,³ and S. SUWAS^{1,4}

1.—Department of Materials Engineering, Indian Institute of Science, Bangalore 560012, India. 2.—Department of Mechanical and Aerospace Engineering, Indian Institute of Technology Hyderabad, Kandi 502285, India. 3.—Boeing Research and Technology - India Center, Bangalore 560016, India. 4.—e-mail: satyamsuwas@iisc.ac.in

This study deals with the evolution of crystallographic texture during secondary processing of aluminium-lithium alloy AA2195 sheets and its effect on the single-point incremental forming (SPIF) process. Significantly different textures were generated in AA2195 alloy sheets by the unidirectional rolling (UDR) and multi-step cross-rolling (MSCR) processes followed by subsequent annealing. The differently textured sheets were then subjected to the SPIF process. For UDR processed sheets, the texture was the strong copper type (Cu-type), whereas in MSCR processed sheets, the texture comprised weak fibres. The UDR samples with strong texture experienced cracking during incremental forming, whereas the MSCR samples could be formed without any cracks. Detailed analyses of the microstructure and texture were performed at various locations on the incrementally formed part to understand the deformation micromechanism at specific locations on the formed component.

INTRODUCTION

Incremental sheet metal forming is a cost-effective die-less forming method to produce complex-shaped components.^{1–6} In this process, tool movement is provided by fully automated computer numerical control (CNC), which enables the manufacturing of more complex components.^{7,8} Formability achieved with the incremental forming method is on the higher side compared with the other conventional forming techniques, such as stamping, die pressing, stretching, deep drawing, etc.^{9,10} The formability of sheet metal, while being formed by incremental forming, exceeds the conventional metal-forming limit diagram.^{11–13} The improved forming efficiency has been attributed to the through-thickness shear strains involved in the process.^{14–17} Shim and Park.³ reported that in the incremental forming process, the total forming strain can be attained before the initiation of localized necking, which renders the process more beneficial than the other traditional sheet-metal-forming processes. Non-monotonic deformation behaviour was experienced during incremental

forming, as revealed by the finite element modelling (FEM) and digital image correlation (DIC) techniques.^{18,19} There are many process variants of the incremental forming process, the most important ones being the single-point incremental forming (SPIF) process and two-point incremental forming (TPIF).^{6,11,14}

Incremental formability of metals and alloys strongly depends on the crystallographic texture of the shapes and the components being formed.¹⁰ It is well known that plastic anisotropy of sheet metal as well as formability can be improved by controlling its crystallographic texture.²⁰ Furthermore, it has been reported that the texture of AA2195 alloy significantly influences its formability.^{21,22}

Texture evolution in FCC materials is a strong function of their stacking fault energy (SFE),^{23,24} and it is well established that materials with high SFE develop a copper-type (Cu-type) texture comprising copper {112}<111>, brass {110}<112> and S {123}<634> (hereafter referred to as Cu, Bs and S) components.²³ In aluminium alloys, the major components of the rolling texture are the Bs, Cu and S components, plus the Cube {100}<001> and Goss

{110}⟨001⟩ components in annealed condition.²⁵ The strong Bs component, if developed in aluminium alloys as a result of thermomechanical processing, leads to anisotropic properties. It is well known that Al-Li alloys are characterized by a strong crystallographic texture with a higher volume fraction of the Bs component.²⁶ When tested for in-plane tensile properties, Al-Li alloys exhibit a lower yield strength at 45°^{21,27} and at 60° to the rolling direction²⁷ compared with that along the rolling direction, which has been attributed to planar slip in Bs-oriented grains.^{21,27} Hence, the Bs component of the texture is regarded as one of the prime causes of anisotropy in Al-Li alloys,²¹ in addition to highly oriented precipitates. Attempts have been made to control the anisotropy in Al-Li-Cu alloys by pre-straining,^{27–29} which could facilitate the precipitation of $T_1(Al_2CuLi)$. However, these methods do not control anisotropy to the desirable extent.^{28,29} Having established that the presence of strong texture in Al-Li alloys restricts the application of these alloys, as strong texture results in anisotropic mechanical properties,²⁶ controlling crystallographic textures is of paramount importance for reducing anisotropy. Though addition of Li is reported to cause a strong Bs texture component,²⁶ Vasudevan et al.³⁰ have reported that the δ' (Al_3Li) precipitates formed in Al-Li alloys homogenize the slip and hence result in the reduction of the Bs component in the overall texture. However, Contrepois et al.³¹ subjected Al alloys with and without Li content to the same thermomechanical processing and concluded that the underlying mechanism during thermomechanical processing is responsible for the strong Bs texture component and not the Li content. Therefore, control of texture by introducing suitable steps in overall processing is highly desirable in the overall scheme of processing. The effect of strain path change on the evolution of texture and mechanical property anisotropy has been studied for many face-centered cubic (FCC) metals and alloys, and it has been established that such a modification in the usual rolling schedule is likely to influence texture formation^{21,28,32–34} and hence the mechanical property anisotropy.

A research study was therefore designed to investigate the evolution of texture after different rolling and annealing conditions. As a quick check of the consequences of the so-obtained textures, incremental forming was employed. The literature available on the effects of starting texture and microstructure for incremental forming is sparse. Therefore, the present work aims to develop a thorough understanding of the role of the starting texture and microstructure on incremental forming. Furthermore, a detailed characterization of the texture and microstructure of the incrementally formed shape was carried out with the aim to understand the deformation micromechanisms in the incrementally formed component.

EXPERIMENTAL PROCEDURE

Materials and Methods

A 12-mm-thick rolled plate of Al-Li alloy, AA2195 (Li: 2.1%, Cu: 4.0%, Mg: 0.4%, Zr: 0.11%, Ag: 0.25%, Al: balance, all in weight percent), was received from Boeing Co., USA. Two samples of 18 mm × 18 mm × 6 mm dimensions were cut out from the plate and subjected to solution treatment at 500°C for 2 h followed by water quenching. The so-obtained slabs were rolled at room temperature following uni-directional rolling (UDR) and multi-step cross rolling (MSCR) to ~80% thickness reduction (true strain $\epsilon_t = 1.6$) leading to 1.2 mm final thickness. The original rolling direction of the as-received alloy was considered as the reference direction. A true strain of $\epsilon_t = 0.1$ per pass was employed during rolling. For cross rolling of the samples, the direction of rolling was altered after every two passes, that is, after a strain interval of $\epsilon_t = 0.2$. The rolled sheets were subsequently annealed for 30 min at 500°C. These annealed sheets were further used for incremental forming.

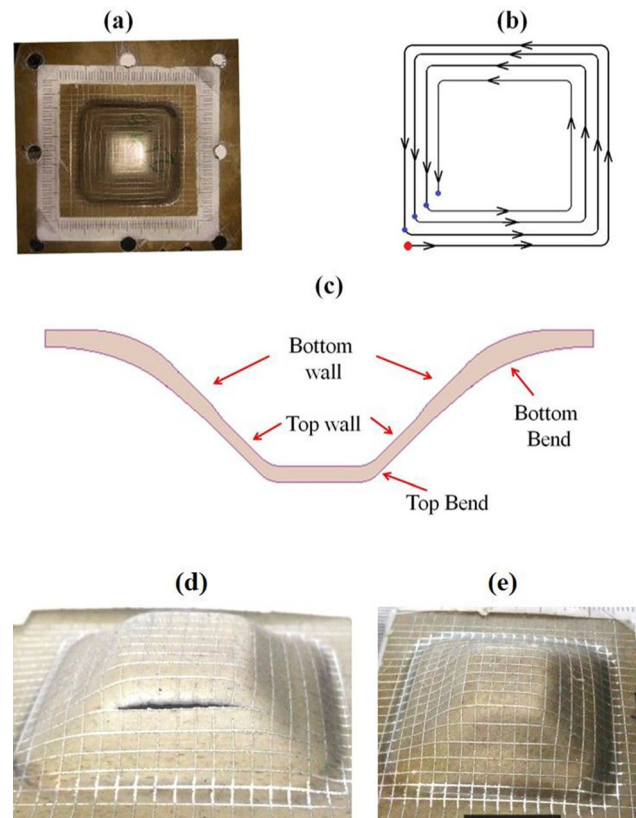


Fig. 1. (a) Photograph of the incrementally formed part, (b) schematic of the tool path employed to form a square-based pyramid-shaped part, (c) cross-sectional view of the formed part showing different regions where the microstructure and texture characterizations were carried out, and (d, e) parts incrementally formed with (i) UDR as the starting material showing crack generated during forming and (ii) MSCR as the starting material showing no crack in the part.

The two differently processed sheets of the Al-Li-Cu alloy (rolled plus annealed) were subjected to the single-point incremental forming (SPIF) process. Figure 1a, b and c show the photograph of the formed part, schematics of the tool path employed and the cross section of the formed part, respectively. The sheet to be formed was clamped between two steel plates with a square opening at the centre to allow the tool to reach the sheet metal and also to allow the part to take the desired shape. The two steel plates were fixed with the help of nuts and bolts at the periphery. The tool, which is an 8.5-mm-diameter steel ball, was allowed to move over the sheet surface along a programmed path to produce the required shape, which was a square-based pyramid in this case (Fig. 1b), using a computer numeric controlled (CNC) machine. The starting point of the forming is indicated by a red circle in Fig. 1b. At the end of every loop in the tool path, the tool moved along the Z axis by 0.1 mm (incremental depth) at the points highlighted with blue circles. Figure 1b shows the formed part at the end of the tool path. The schematic representation in Fig. 1c shows the cross-sectional view of the incrementally formed part. The incrementally formed parts with starting UDR and MSCR processed sheets are shown in Fig. 1d and e. A crack was observed in the part formed out of the UDR processed starting material, while the part formed out of the MSCR processed sheet had no cracks. In the former case, cracks were observed at a depth of 9 mm, whereas in the latter, no crack was observed up to 10 mm depth. The wall angle was $\sim 45^\circ$ for both cases.

Characterization

A detailed characterization of the microstructure, microtexture as well as bulk texture has been carried out using electron backscatter diffraction (EBSD) and x-ray diffraction techniques. Microstructural characterization was done using a scanning electron microscope (SEM) equipped with an electron backscatter diffraction (EBSD) facility. All the EBSD scans were recorded on the transverse (TD) plane (across thickness) of the rolled sheets. Measured EBSD scan sizes were approximately $150 \mu\text{m} \times 150 \mu\text{m}$ for all the samples. For EBSD measurements, the rolled samples were mechanically polished followed by electro-polishing. The step size for all the measurements was kept constant ($0.4 \mu\text{m}$). The data analyses were carried out using TSL-OIMTM software.

Bulk textures of the rolled sheets were measured using a four-circle x-ray texture goniometer based on Schultz reflection geometry using a Bruker D8 Discover diffractometer with a Co $K\alpha$ ($\lambda = 0.1791 \text{ nm}$) target. Four incomplete pole figures, viz. (111), (200), (220) and (311), were measured with the sample frame of reference parallel to the rolling plane. All the measurements were carried out in the range of χ ($\chi = 0-75^\circ$) with a step size of

5° and exposure time of 5 s. Three-dimensional orientation distribution functions (ODFs) were calculated from the four x-ray measured pole figures using Labotex software.

For the incrementally formed parts, the microstructure and microtexture were characterized at four locations, namely TopW, BotW, TopBend and BotBend, as shown in Fig. 1c.

Hardness profiles were obtained across the incrementally formed part, from the base of the pyramid to the top, using a Vickers microhardness tester. The incrementally formed part was sectioned and measurements were carried out at the cross section of the sheet. A 300-gmf load and 15-s dwell time were used for the hardness measurement. Average hardness was estimated from the five measurements.

RESULTS AND DISCUSSION

Microstructure and Texture of the Starting Material

Figure 2a and b shows the microstructure and texture of the as-received AA2195 alloy before subjecting it to UDR and MSCR modes of rolling. The microstructure consists of elongated grains. The texture of the starting material, as revealed by the (111) pole figure, depicts a strong Cu-type texture. Textures of the uni-directionally rolled and multi-step cross-rolled samples are shown in Fig. 2c and d. The texture of the cross-rolled sample is weaker than that of the uni-directionally rolled sample.

Figure 3a and b shows the EBSD-generated microstructures for the UDR and MSCR samples, respectively, after annealing. A mixture of elongated plus equiaxed grains is observed in the microstructure of the UDR sample, while the microstructure is fully equiaxed for the MSCR sample. For the MSCR sample, the grains are relatively coarser. The textures of these materials are shown in Fig. 3c and d, using the orientation distribution function (ODF). Strong texture can be clearly noticed for the UDR sample, whereas the texture of the MSCR sample is relatively very weak. In FCC materials, it has been reported that MSCR produces a weaker texture than UDR.³² In the UDR sample, strong Bs and S components are observed in the $\Phi_2 = 0^\circ$ and 65° sections of the ODF. In the literature, it has been well documented that the Goss, Bs, Cu and Cube texture components significantly influence the Lankford parameter.^{35,36} The Lankford parameter is the strain or strain rate ratio between the width to thickness direction. Physically, it defines the capacity to resist thinning of the sheet metal during forming.³⁵

Many investigations pertaining to the texture evolution in FCC materials have clearly indicated that SFE is the major factor influencing the texture evolution in FCC materials. Hirsch and Lücke,³⁷⁻⁴⁰ Ray,⁴¹ Engler⁴² and later on Madhavan

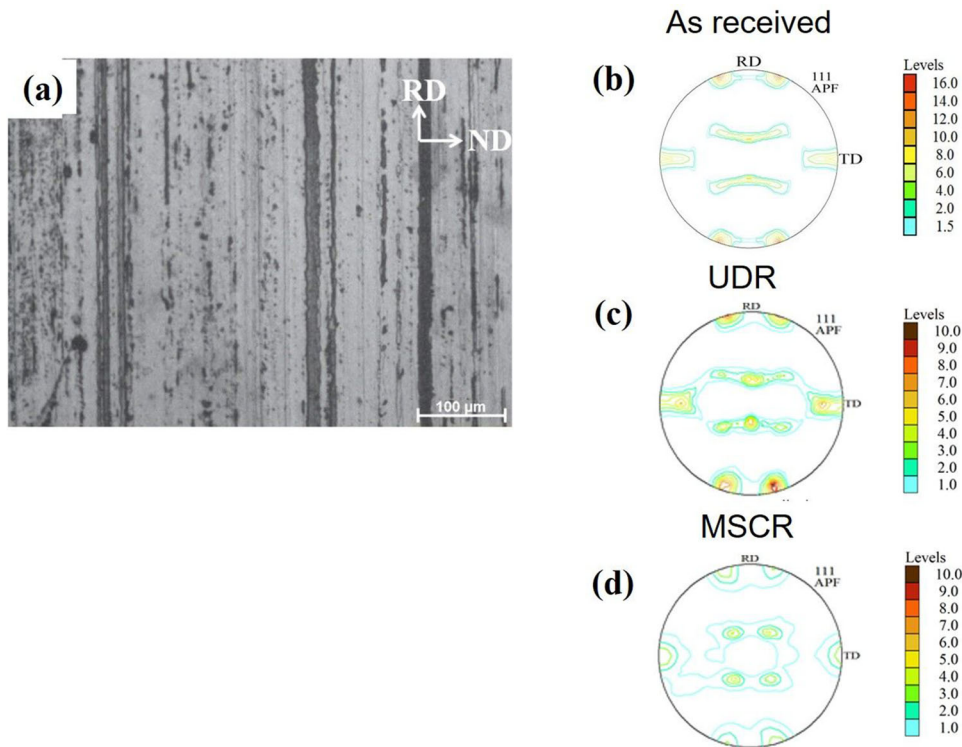


Fig. 2. (a) Microstructure of the material before subjecting it to UDR and MSCR modes of rolling and (b) (111) pole figure depicting a strong Cu-type texture; (c, d) (111) pole figure of uni-directionally rolled (UDR) and cross rolled (MSCR) samples, respectively.

et al.^{23,24,43–45} studied the stacking fault energy-dependent texture evolution in FCC materials. In the present investigation, texture evolution broadly follows the trend expected for Al alloys, which are characterized by high SFE. In addition, a number of reports are available elucidating the strain path dependence of texture.^{23,32,33,46–51} Deformation textures in unidirectional cold rolling of FCC metals comprise α -fibre, which connects the Goss orientation to the Bs orientation, and β -fibre, which connects the Cu orientation to the Bs orientation via S orientation.^{37,40,42} The deformation textures of cross-rolled FCC materials significantly differ from those of uni-directionally rolled specimens.^{32,46,51}

Stability or instability of orientations with respect to the deformation frame of reference is responsible for the texture components observed in cross rolling. The stability of various texture components is reported in the literature for unidirectional rolling.^{52–54} It is also reported that cross rolling leads to the development of a strong α -fibre and results in the reduction of the intensities of the β -fibre from the former frame of reference due to the instability of these orientations in the new sample frame.^{47,50,55} The stability of the Bs component is well reported for unidirectional rolling.⁵¹ The stable Bs component loses its stability when rolled along 90° to the earlier rolling direction. Both of these components rotate; however, their rotation is complimentary as the rotations are confined mostly to the $\langle 110 \rangle$ ND zones during cross rolling. This

results in a rotated Bs component as the main texture component in the cross-rolled material.⁵¹

In case of unidirectional rolling of the FCC materials, the volume fraction of the Cube component progressively decreases with strain because of its metastability during uni-directional rolling. Dillamore and Katoh⁵⁶ reported that during their rotation to the stable end orientation the crystallites pass through the Cube component during rolling. Hong et al.⁵¹ explained the formation of a strong Cube component during cross rolling. They showed by calculations that the Cube components are metastable for rolling along both the RD and TD directions. As a result, most crystal orientations rotate 'to and fro' through the Cube orientation during alternate passes of cross rolling, increasing its chances to exist during cross rolling.

The recrystallization textures of both the uni-directionally rolled and cross-rolled samples are shown in Fig. 3. In case of UDR plus annealed samples, the recrystallization texture retains its deformation texture components (Fig. 2c and d). Recrystallization textures are weaker in the cross-rolled sample in line with their deformation texture. Huh et al.⁵⁰ also showed the efficient randomization of recrystallization texture after cross rolling in an aluminium AA5182 sheet. The randomization of texture depends on the cross-rolling schedule and relative texture component rotation during deformation.⁵² The recrystallization of deformed materials proceeds by the nucleation and subsequent grain

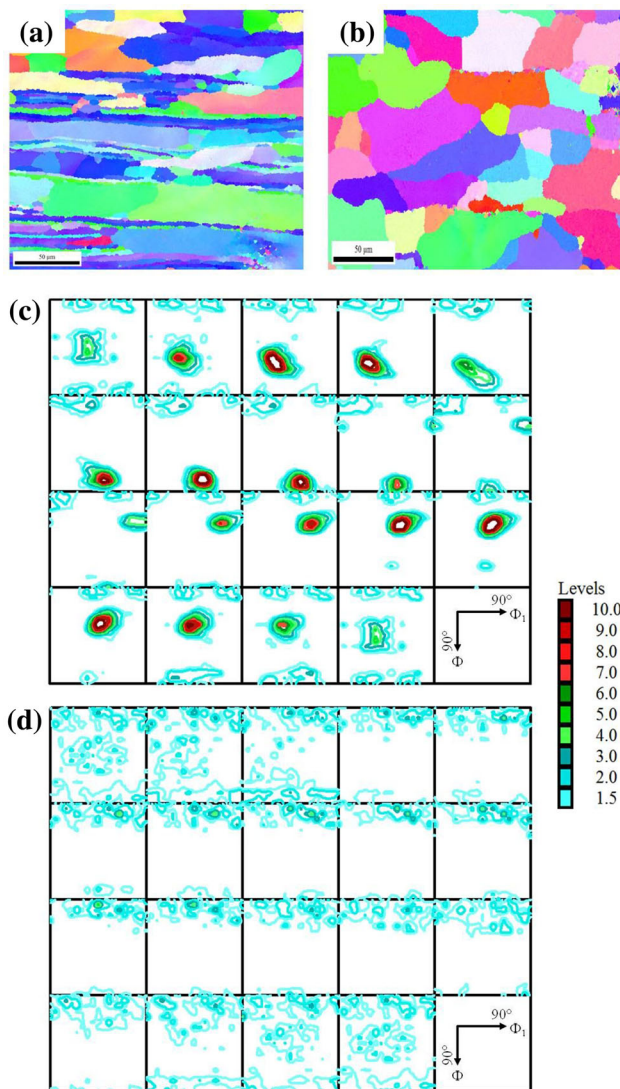


Fig. 3. (a, b) EBSD-generated recrystallized microstructure of rolled plus annealed sample: (a) UDR and (b) MSCR; (c, d) ODF representing the textures of (c) UDR and (d) MSCR samples.

growth in the deformed microstructure;⁵⁷ hence, the nucleation and grain growth responses of cross-rolled materials have a significant effect on texture randomization during annealing. In the present case, the deformation texture components are destroyed in the cross-rolled plus annealed samples. A weak cube fibre type texture development was observed in the cross-rolled and annealed sample (Fig. 3). In the present case, the recrystallization texture development is influenced by oriented growth theory, the recrystallized grains or nuclei follow an orientation relationship of $30^\circ\langle 111 \rangle$ with the $\{110\}\langle 755 \rangle$ deformation orientation. These oriented grains grow fast and eventually dominate the main recrystallization texture.⁵¹ Lücke⁵⁸ showed a $40^\circ\langle 111 \rangle$ orientation relationship with the deformed matrix, which has the highest growth rate. Grains that are favourably oriented for such an orientation relationship with a

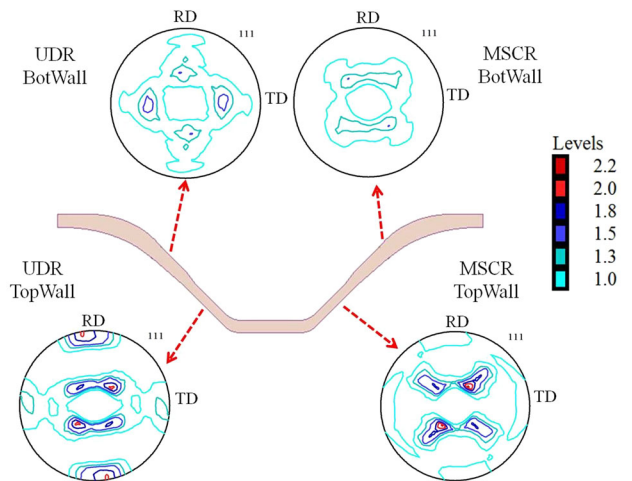


Fig. 4. $\langle 111 \rangle$ Pole figure showing texture at two different locations of incrementally formed parts from the sheets processed by the UDR and MSCR routes.

strong component of rolling texture form recrystallization components.

Texture Evolution During Incremental Forming

Figure 4 shows the texture at two different locations for the incrementally formed parts made from the UDR and MSCR processed sheets. The texture is weak at the BotW and strong at the TopW location for both samples. The $\langle 111 \rangle$ pole figure shows different textures at the two locations for the parts produced from the two different starting materials. In case of the IF part obtained from the UDR processed sheet, the $\langle 111 \rangle$ pole figure depicts a weak cube fibre at BotW and strong Bs, Cu and S components at the TopW locations. However, in case of the IF part formed from the MSCR processed sheet, a weak cube texture has been noticed at the BotW, and strong cube plus weak Bs components are detected at the TopW location.

For a more complete depiction of texture, the orientation distribution function (ODF) has been calculated and plotted in Euler space. Figure 5 shows the ODFs for the incrementally formed (IF) parts obtained from the UDR and MSCR sheets at two different locations. The texture is weaker at the BotW location than at the TopW location. However, comparing the parts formed from the UDR and MSCR sheet, the texture is stronger in the former. At the BotW location, the texture comprises cube fibres. The ODF clearly reveals a Cu-type texture at the TopW location of the IF part formed from the UDR sheet where the intensity maxima are located at the Bs, Cu and S positions. On the other hand, for the IF part formed from the MSCR sheet, a texture with strong cube and weak Bs components develops at the TopW location. During incremental forming, mainly two types of forces are being applied on the

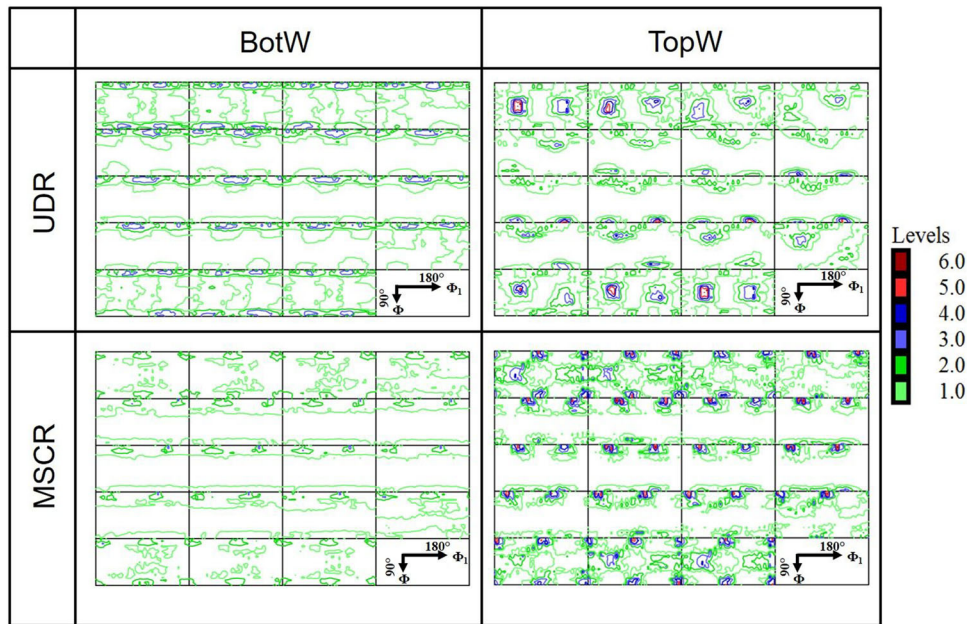


Fig. 5. Deformation texture of the as-formed component at two different locations (BotW and TopW) with starting materials as sheets processed by the UDR and MSCR routes. Texture is represented by $\Phi_2 = 0^\circ\text{--}90^\circ$ sections of the ODF with 5° increment.

plate, compressive and shear forces. Although it is difficult to quantify these two forces, in general the shear force varies at different locations in the formed part. At the BotW location, deformation is comparatively less and the texture of the starting material is retained. On the contrary, at the TopW position, the texture is relatively stronger because of the higher degree of plastic deformation imparted during incremental forming. Through-thickness shear strain is one of the main mechanisms reported for efficient formability in incremental forming.^{14,15} A strong Goss texture component forms in aluminium alloys during incremental forming, which is three times stronger at the centre than at the surface.³⁵ The through thickness texture variation has positive influence on Lankford parameter.⁵⁹

Microstructural Evolution During Incremental Forming

A detailed microstructural characterization of the entire IF part was carried out by EBSD. Figure 6 shows the inverse pole figure (IPF) maps of the IF part at different locations. Microstructures are presented for the four locations, BotBend, BotW, TopBend and TopW. In the IF part formed from the UDR sheet, all the microstructures are characterized by an elongated grain structure with a high aspect ratio, except at the TopBend location. The microstructure at the TopBend location shows a mixture of elongated and equiaxed grains, with a smaller fraction of the latter. The average grain sizes for the starting materials were measured to be $33 \pm 9 \mu\text{m}$ and $35 \pm 3 \mu\text{m}$ for the UDR and MSCR samples, respectively. After incremental forming, the average grain sizes for the UDR sample at

BotBend, BotW, TopBend and TopW were measured as $24 \pm 5 \mu\text{m}$, $30 \pm 8 \mu\text{m}$, $22 \pm 5 \mu\text{m}$ and $16 \pm 3 \mu\text{m}$, respectively. On the other hand, after forming, the average grain sizes for the MSCR sample at BotBend, BotW, TopBend and TopW were estimated as $33 \pm 5 \mu\text{m}$, $35 \pm 8 \mu\text{m}$, $26 \pm 5 \mu\text{m}$ and $20 \pm 3 \mu\text{m}$, respectively.

The microstructures from all the locations of the IF part formed from the MSCR sheet at the bottom bend, bottom wall and top wall consist of a mixture of equiaxed and elongated grains. The fraction of elongated grains is less in this case than the part formed from the UDR sheets.

The EBSD data were further analyzed by calculating the kernel average misorientation (KAM) and misorientation distribution plots (Fig. 7). The KAM data represent the development of intragranular misorientation during deformation due to accommodation of geometrically necessary dislocations (GNDs). In the present analysis, the first nearest neighbour approximation has been considered for KAM calculation. In the misorientation distribution plot, the misorientation range $2^\circ \leq \theta \leq 15^\circ$ is considered low-angle grain boundaries (LAGBs), and $\theta \geq 15^\circ$ is considered as high-angle grain boundaries (HAGBs). The KAM and misorientation distributions are presented in Fig. 7a and b for the IF part formed from the UDR sheet. The figure shows a very high LAGB fraction in case of the TopBend and TopW locations compared with the base material, BotBend and BotW sections. The maxima of LAGBs are located at $3\text{--}10^\circ$ and HAGBs are located at $\sim 57^\circ$ misorientation. A large LAGB fraction indicates the accumulation of more strain or sub-grain formation. The highest KAM value is

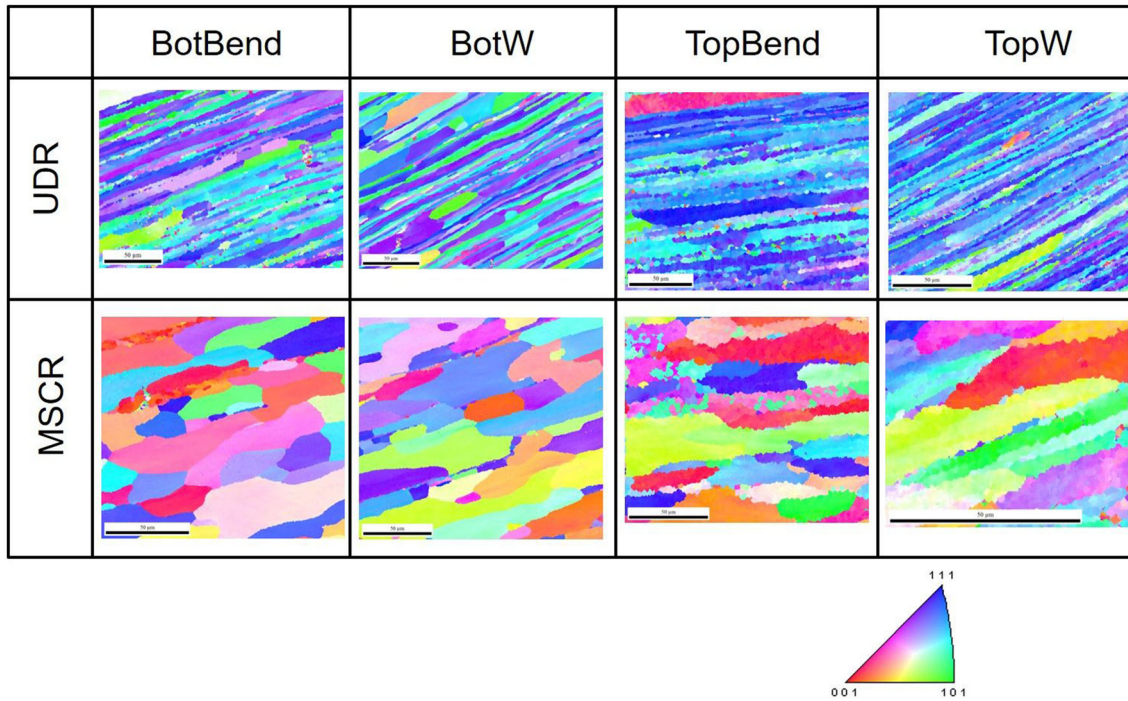


Fig. 6. EBSD-generated microstructure of UDR and MSCR samples after incremental forming for the BotBend, BW, TopBend and TW locations.

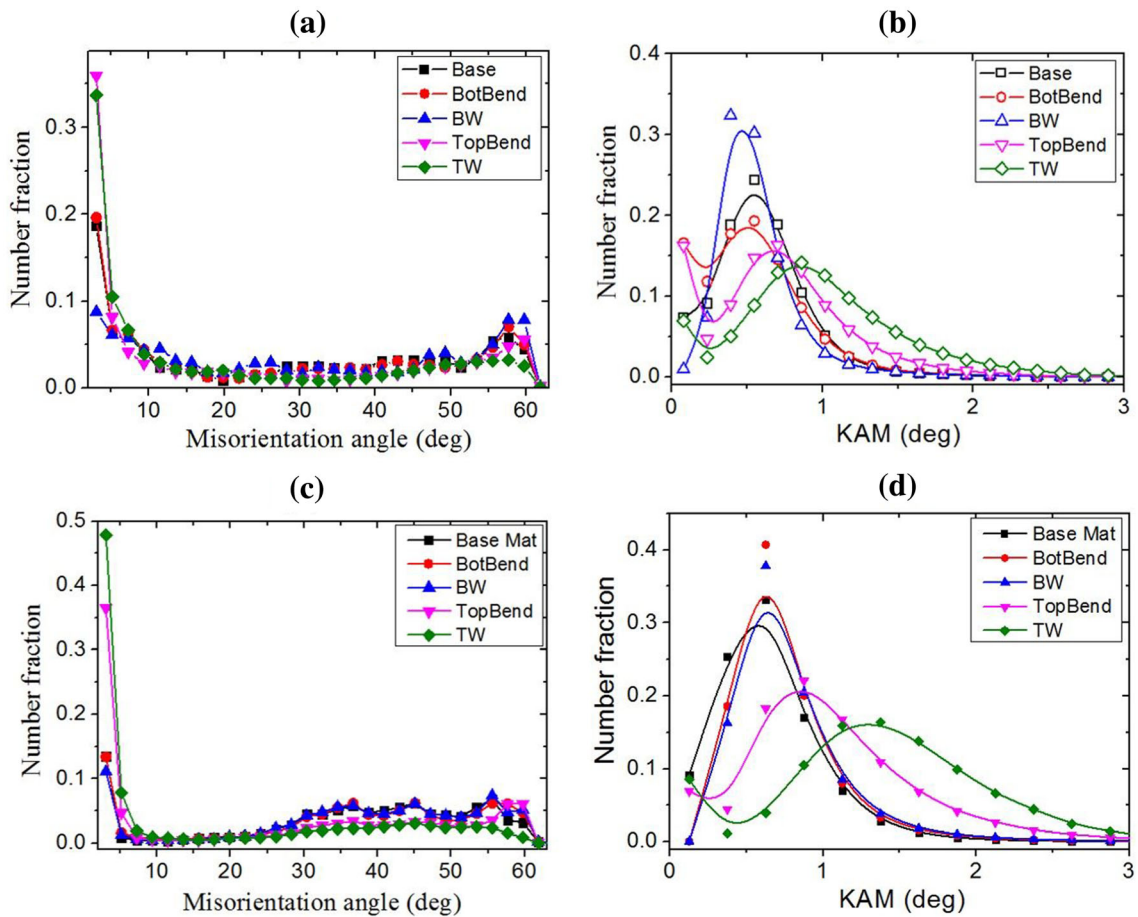


Fig. 7. Misorientation distribution and KAM plots for the base material and different sections (bottom bend, bottom wall, top bend and top wall) of the incrementally formed parts; (a, b) for the IF part formed from the UDR sheet and (c, d) for the IF part formed from the MSCR sample.

for the TopBend and TopW sections, which implies higher intragranular strain accumulation during forming.

The KAM and misorientation distribution for the IF parts formed from the MSCR sheets (Figs. 7c and d) show a higher LAGB fraction for the TopBend and TW locations compared with the base material, BotBend and BotW sections. In both the IF parts (UDR and MSCR as starting sheets) maximum strain accumulation takes place at the TopBend and TopW locations. This observation leads to the understanding that the level of deformation is similar in both IF parts, although the texture and microstructure of the starting sheet materials were different. However, the part formed from the UDR sheet was susceptible to the formation of cracks during IF. This can be related to the texture-dependent anisotropic yield phenomenon. The IF sample with UDR sheets reaches yielding earlier because of its texture and causes early failure, whereas the texture of MSCR processed sample helps improve formability. Inal et al.²⁰ reported anisotropic hardening and its impact on the Lankford parameter and yield locus in AA5754 aluminium sheets. Anisotropic hardening due to the starting texture plays a dominating role in enhanced formability. The weaker starting texture in the MSCR sheets favours improved formability.

Hardness Variation After Incremental Forming

Figure 8 shows the microhardness data at different locations for UDR and MSCR sheets before and after incremental forming. The plot displays a significant increase in hardness for both samples with respect to the base material. The highest hardness is observed at the TopW and BotW locations compared with the TopBend and BotBend locations. A clear transition in hardness is observed at the TopBend and BotBend locations. However, the difference in hardness is small between the UDR and MSCR starting materials, which indicates

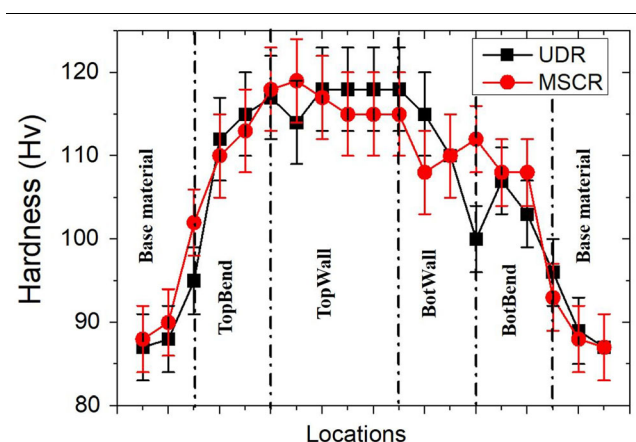


Fig. 8. Microhardness values across the cross section of incrementally formed components.

that the cracks after incremental forming were not due to excessive strain hardening during processing but due to the texture of the starting material. Shrivastava and Tandan¹⁰ reported that biaxial strain at early stages of forming causes the material to be more susceptible to failure. In the present case, since hardness variation across the component is nearly similar, the failure due to the strain localization mechanism can be eliminated.

CONCLUSION

In the present investigation, an attempt has been made to understand the role of starting texture and microstructure in the incremental forming of the aerospace-grade Al-Li 2195 alloy. Two different rolling processes were adopted to get two different textures, in one case a very strong starting texture and in the other a weak starting texture. The post forming texture and microstructural analyses of the experimental results led to the following key conclusions:

1. Significant texture weakening is observed after cross rolling, which is attributed to continuous destabilization of texture component during intermediate changes in the strain path and inhomogeneous slip activity. In case of UDR plus annealed samples, the recrystallization texture retains its deformation texture components; however, deformation texture components are destroyed in cross-rolled plus annealed samples.
2. Crack formation is observed in the sample with UDR processing; however, no cracks are observed in the samples with MSCR processing, which can be attributed to the starting texture. As the starting texture is very strong in UDR processed samples, cracks form during incremental sheet forming.
3. Starting microstructural features are comprised of elongated grains in the samples processed through the UDR route compared with the MSCR route. The starting microstructure with equiaxed grains is suitable for improved formability. An elongated microstructure is observed in both the incrementally formed UDR and MSCR samples but the grain aspect ratio is very high in the UDR sample. In this case, the higher grain aspect ratio during forming appeared to be detrimental to incremental forming. This clearly manifests that the starting microstructure has a significant role in incremental forming.
4. Microhardness variation across the incrementally formed component reveals very similar strain hardening in both samples, which implies that localized strain hardening does not play a large role in cracking. The starting texture plays a key role in crack-free processing.

ACKNOWLEDGEMENTS

The authors acknowledge Boeing Co. for funding this work. The extensive use of microscopes at the Advanced Facility of Microscopy and Microanalysis (AFMM) facility and XRD at the institute's x-ray facility, Indian Institute of Science, Bangalore is also acknowledged.

REFERENCES

- G. Fan, L. Gao, G. Hussain, and Z. Wu, *Int. J. Machine Tools Manuf.* 48, 1688 (2008).
- T. Kim and D. Yang, *Int. J. Mech. Sci.* 42, 1271 (2000).
- M.-S. Shim and J.-J. Park, *J. Mater. Process. Technol.* 113, 654 (2001).
- X.H. Cui, J.H. Mo, J.J. Li, J. Zhao, Y. Zhu, L. Huang, Z.W. Li, and K. Zhong, *J. Mater. Process. Technol.* 214, 409 (2014).
- L. Edward, *Apparatus and process for incremental dieless forming*, Uniter States Patent 3342051 (1967). Edward, Leszak, <http://www.freepatentsonline.com/3342051.html>.
- J. Jeswiet, J.R. Dufloy, and A. Szekeres, *Adv. Mater. Res.* 6–8, 4496 (2005).
- W. Emmens, G. Sebastiani, and A.H. van den Boogaard, *J. Mater. Process. Technol.* 210, 981 (2010).
- J. Cao, Y. Huang, N.V. Reddy, R. Malhotra, and Y. Wang, *Incremental sheet metal forming: Advances and challenges. 1967–1982*. Paper presented at 9th International Conference on Technology of Plasticity, ICTP 2008, Gyeongju, Republic of Korea (2008).
- C. Wong, T. Dean, and J. Lin, *Int. J. Machine Tools Manuf.* 43, 1419 (2003).
- P. Shrivastava and P. Tandon, *J. Mater. Process. Technol.* 266, 292 (2019).
- B. Taleb Araghi, A. Göttmann, M. Bambach, G. Hirt, G. Bergweiler, J. Dietrich, M. Steiners, and A. Saeed-Akbari, *Prod. Eng.* 5, 393 (2011).
- H. Iseki, An experimental and theoretical study of a forming limit curve in incremental forming of sheet metal using spherical roller. *Proc. Met. Form* 557 (2000).
- W. Emmens and A.H. van den Boogaard, *J. Mater. Process. Technol.* 209, 3688 (2009).
- K.U. Yazar, S. Mishra, K. Narasimhan, and P.P. Date, *Int. J. Adv. Manuf. Technol.* 101, 2355 (2019).
- J. Allwood, D. Shouler, and A.E. Tekkaya, *Key Eng. Mater.* 549, 372 (2007).
- R. Esmaeilpour, H. Kim, T. Park, F. Pourboghraat, and B. Mohammed, *Int. J. Mech. Sci.* 133, 544 (2017).
- F. Maqbool and M. Bambach, *Int. J. Mech. Sci.* 136, 279 (2018).
- P. Flores, L. Duchene, C. Bouffloux, T. Lelotte, C. Henrard, N. Pernin, A.V. Bael, S. He, J. Dufloy, and A.M. Habraken, *Int. J. Plast.* 23, 420 (2007).
- Y. Li, W.J. Daniel, and P.A. Meehan, *Int. J. Adv. Manuf. Technol.* 88, 255 (2017).
- K. Inal, R.K. Mishra, and O. Cazacu, *Int. J. Solids Struct.* 47, 2223–2233 (2010).
- R. Crooks, Z. Wang, V.I. Levit, and R.N. Shenoy, *Mater. Sci. Eng., A* 257, 145 (1998).
- K. Jata, S. Panchanadeswaran, and A. Vasudevan, *Mater. Sci. Eng. A* 257, 37–46 (1998).
- R. Madhavan, R. Kalsar, R.K. Ray, and S. Suwas, *IOP Conf. Ser. Mater. Sci. Eng.* 82, 012031 (2015).
- R. Madhavan, R. Ray, and S. Suwas, *Philos. Mag.* 96, 3177 (2016).
- S. Roy, D. Satyaveer Singh, S. Suwas, S. Kumar, and K. Chattopadhyay, *Mater. Sci. Eng. A* 528, 8469 (2011).
- R.J. Rioja and J. Liu, *Metall. Mater. Trans. A* 43, 3325 (2012).
- N.J. Kim and E.W. Lee, *Acta Metall. Mater.* 41, 941 (1993).
- E.W. Lee, P.N. Kalu, L. Brandao, O.S. Es-Said, J. Foyos, and H. Garmestani, *Mater. Sci. Eng., A* 265, 100 (1999).
- O.S. Es-Said, C.J. Parrish, C.A. Bradberry, J.Y. Hassoun, R.A. Parish, A. Nash, and N.C. Smythe, et al., *J. Mater. Eng. Perform.* 20, 1171 (2011).
- A. Vasudevan, M. Przystupa, and W. Fricke Jr, *Mater. Sci. Eng., A* 196, 1 (1995).
- Q. Contrepolis, C. Maurice, and J. Driver, *Mater. Sci. Eng., A* 527, 7305 (2010).
- N. Gurao, S. Sethuraman, and S. Suwas, *Mater. Sci. Eng., A* 528, 7739 (2011).
- S. Suwas, A.K. Singh, K. Narasimha Rao, and T. Singh, *Z. Metallkunde* 94, 1313 (2003).
- P. Kalu and L. Zhang, *Scr. Mater.* 39, 175 (1998).
- X.Y. Wen, Z.D. Long, W.M. Yin, T. Zhai, Z. Li, and S.K. Das, Texture evolution in continuous casting AA5052 aluminum alloy hot band during equi-biaxial stretching, in *Aluminum Wrought Products for Automotive, Packaging, and Other Applications—The James Morris Honorary Symposium, TMS* (2006).
- O. Engler and J. Aegerter, *Mater. Sci. Eng., A* 618, 663 (2014).
- J. Hirsch and K. Lücke, *Acta Metall.* 36, 2863 (1988).
- J. Hirsch and K. Lücke, *Acta Metall.* 36, 2883 (1988).
- J. Hirsch, K. Lücke, and M. Hatherly, *Acta Metall.* 36, 2905 (1988).
- J. Hirsch, E. Nes, and K. Lücke, *Acta Metall.* 35, 427 (1987).
- R. Ray, *Acta Metall. Mater.* 43, 3861 (1995).
- O. Engler, J. Hirsch, and K. Lücke, *Acta Metall.* 37, 2743 (1989).
- R. Madhavan, R. Ray, and S. Suwas, *Acta Mater.* 74, 151 (2014).
- R. Madhavan, R. Ray, and S. Suwas, *Acta Mater.* 78, 222 (2014).
- R. Madhavan and S. Suwas, *Philos. Mag. Lett.* 94, 548 (2014).
- S. Suwas, A.K. Singh, K. Narasimha Rao, and T. Singh, *Z. Metallkunde* 93, 918 (2002).
- S. Suwas and A. Singh, *Mater. Sci. Eng., A* 356, 368 (2003).
- S. Suwas and N. Gurao, Development of microstructures and textures by cross rolling. *Comput. Mater. Process.* 3, 81–106 (2014).
- S.H. Kim, H.G. Kang, M.Y. Huh, and O. Engler, *Mater. Sci. Eng. A* 508, 121 (2009).
- M. Huh, S. Cho, and O. Engler, *Mater. Sci. Eng., A* 315, 35 (2001).
- S.-H. Hong and D.N. Lee, *J. Eng. Mater. Technol.* 124, 13 (2002).
- J. Kallend and G. Davies, *Philos. Mag.* 25, 471 (1972).
- I.L. Dillamore, P.L. Morris, C.J.E. Smith, and W.B. Hutchinson, *Proc. R. Soc. Lond. A* 1756, 1447 (1972).
- I. Dillamore, E. Butler, and D. Green, *Met. Sci. J.* 2, 161 (1968).
- O. Engler and K. Lücke, *Texture Stress Microstruct.* 14, 727 (1991).
- I. Dillamore and H. Katoh, *Met. Sci.* 8, 73 (1974).
- F. Humphrey and M. Hatherly, *Recrystallization and Related Annealing Phenomena* (Oxford: Pergamon, ISBN, 1996).
- K. Lücke, *Can. Metall. Q.* 13, 261 (1974).
- M. Ghosh, A. Miroux, and L. Kestens, *J. Alloys Compd.* 619, 585 (2015).

Publisher's Note Springer Nature remains neutral with regard to jurisdictional claims in published maps and institutional affiliations.